ACS APPLIED MATERIALS & INTERFACES

Research Article

www.acsami.org

Bioinspired Templating Synthesis of Metal–Polymer Hybrid Nanostructures within 3D Electrospun Nanofibers

Ho Yeon Son,[†] Ji Hyun Ryu,[‡] Haeshin Lee,*[,‡,§,⊥] and Yoon Sung Nam*[,†,⊥]

[†]Department of Materials Science and Engineering, [‡]Graduate School of Nanoscience & Nanotechnology, [§]Department of Chemistry, and [⊥]KAIST Institute for NanoCentury and BioCentury, Korea Advanced Institute of Science and Technology, 291 Daehak-ro, Yuseong-gu, Daejeon, 305-701, Republic of Korea

Supporting Information

ABSTRACT: Novel metal nanostructures immobilized within three-dimensional (3D) porous polymeric scaffolds have been utilized for catalysts and biosensors. However, efficient, robust immobilization of the nanostructures both outside and inside of the 3D scaffolds is a challenging task. To address the challenge, we synthesized a redox-active polymer, catechol-grafted poly(vinyl alcohol), PVA-*g*-ct. The grafted catechol is inspired by the adhesion mechanism of marine mussels, which facilitates binding and reduction of noble metal ions. Electrospinning the PVA-*g*-ct polymer results in highly open porous, 3D nanostructures, on which catechol mediates the spontaneous reduction of silver ions to solid silver nanocubes at an ambient temperature. Yet, gold and platinum ions are partially reduced and complexed with the nanofiber template, requiring an additional thermal treatment for complete reduction into solid metal nanostructures. Furthermore, silver–gold and silver–platinum hybrid nanostructures are generated by sequential treatments with metal ion precursor solutions of each. This study suggests that catechol-grafted polymer nanofibers are an attractive reactive template for the facile synthesis and immobilization of noble metal nanostructures within a 3D porous matrix for the potential applications to sensors, catalysis, and tissue engineering.

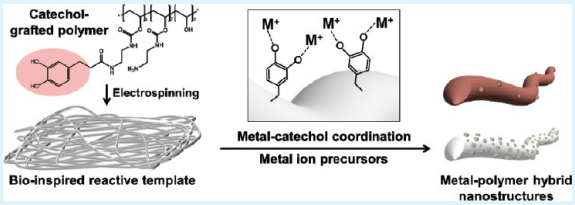

KEYWORDS: *catechol, electrospun nanofibers, poly(vinyl alcohol), metal reduction, metal nanostructures*

1. INTRODUCTION

Recently, there has been increasing attention directed toward the synthesis and assembly of functional inorganic and organic–inorganic hybrid nanostructures.[1,2] In particular, noble metal nanoparticles have been investigated extensively as an active material for biosensors and catalytic systems and for use in electronic, electrochemical, and optical devices.[3−5] However, the structural instability of metal nanoparticles (e.g., aggregation) followed by changes in their intrinsic properties often narrows the range of their applications. To prevent such structural changes, porous materials have been employed as a support to immobilize metal nanoparticles.[3] Porous polymeric materials are attractive as a template for metal nanoparticles due to their tunable three-dimensional (3D) architectures and versatile surface modification potential. A variety of fabrication techniques have been developed for3D porous polymeric materials, including phase separation, salt leaching, gas foaming, colloidal templating, and electrospinning.[6−12] Electrospinning is particularly attractive because of the feasible scale-up production that becomes possible with the facile optimization of the pore sizes, porosities, and mechanical properties.[11,12]

Several methods have been investigated to synthesize and immobilize metal nanostructures using electrospun polymer nanofibers as a template. For instance, metal nanoparticle–polymer hybrid nanofibers can be prepared by electrospinning metal nanoparticles suspended in a polymer solution.[13] Metal nanoparticles can also be directly deposited on surface-modified polymer nanofibers via electrostatic interactions and/or interfacial hydrogen bonding.[14−17] These methods require the synthesis of metal nanoparticles prior to the fabrication of metalized nanofiber structures. Alternatively, metal nanostructures can be synthesized on the surface of electrospun nanofibers through the thermal or chemical reduction of metal precursor ions.[18,19] The templated synthesis of metal nanostructures is generally carried out by adding highly reactive and toxic reducing agents or under relatively harsh conditions (e.g., at a high temperature or under an extreme vacuum).

Recently, 3,4-dihydroxy-L-phenylalanine (DOPA) and its polymeric forms, found in mussel adhesive proteins, have received increasing amounts of attention as regards bioinspired surface modifications as these materials can be used to coat various organic and inorganic materials.[20−26] It is known that the coexistence of the catechol moiety of DOPA and the primary amine group of lysine is crucial for strong mussel adhesion in an aqueous milieu.[20] Interestingly, some metal ions can be reduced by the oxidation of catechol due to its relatively low redox potential (+530 mV vs a normal hydrogen electrode (NHE) at pH 7).[27] This reduction power may be high enough to induce a chemical reduction of noble metal ions though the

Received: April 26, 2013
Accepted: June 13, 2013
Published: June 13, 2013

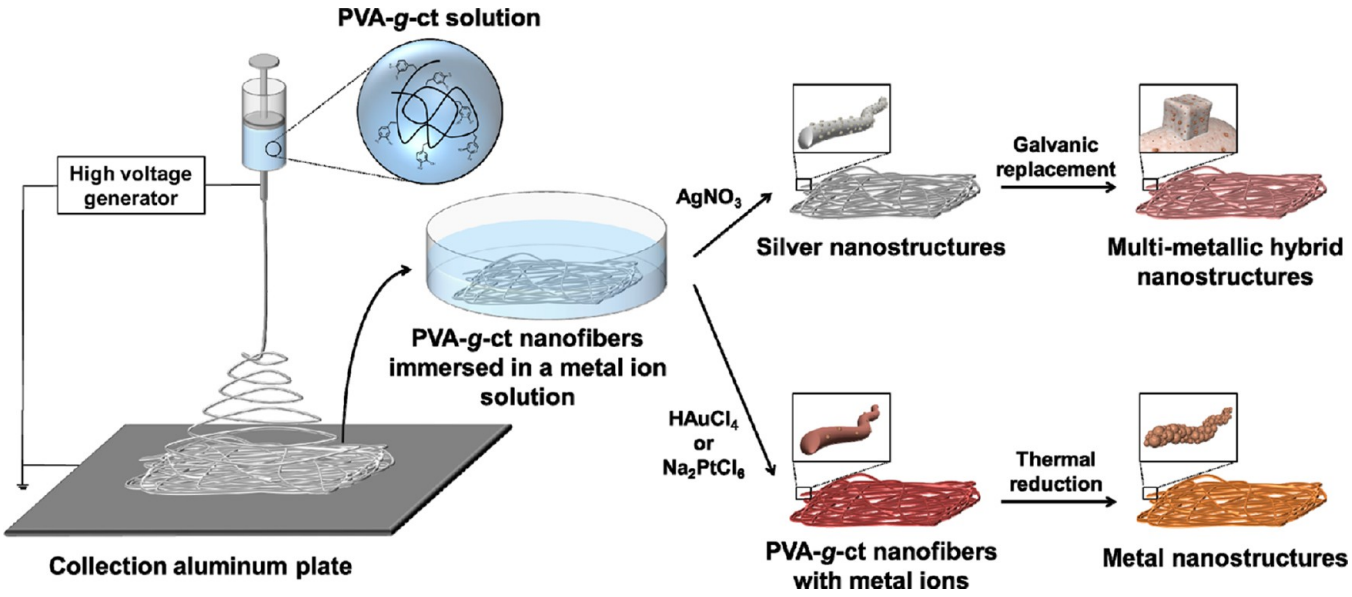

Figure 1. Schematic illustration of the mussel-inspired templating synthesis of noble metal nanostructures on the electrospun PVA-*g*-ct nanofibers.

reaction kinetics, and the conversion efficiency may depend on the experimental conditions.[25,28−31]

Here, we introduce a facile templating method to synthesize and assemble noble metal nanostructures using electrospun catechol-grafted poly(vinyl alcohol) (PVA) nanofibers as a chemically functional template. PVA is known to act as a capping agent during the formation of metal nanoparticles.[32] The hydroxyl groups of PVA can also be used to introduce various functional groups through chemical modifications.[33,34] In this work, 3,4-dihydroxyhydrocinnamic acid (HCA) was chemically grafted onto PVA to produce catechol-grafted PVA, denoted as "PVA-*g*-ct". PVA-*g*-ct was electrospun into nanofibers, and the prepared PVA-*g*-ct nanofibers were used as a chemically reactive template for the reduction of metal ions into solidmetal nanostructures. The prepared PVA-*g*-ct nanofibers were simply immersed intoa metal ion solution (i.e., Ag^{+}, Au^{3+}, and Pt^{4+}) at an ambient temperature to generate metal ion-catechol complexes on the nanofibers, with their subsequentspontaneousreduction into highly porous, 3D metal−polymer hybridmaterials (Figure 1). Our mussel-inspired chemically reactive nanofibers can provide a very useful platform for the facile templating synthesis of noble metal nanostructures within porous 3D structures for various applications. In particular, to the best of our knowledge, this is the first report on the catechol-mediated synthesis of platinum nanostructures, which are widely used for a wide range of catalysis.

2. EXPERIMENTAL SECTION

2.1. Chemicals and Materials. PVA (M_w = 85−124 kDa, 98−99% hydrolyzed), 1,1′-carbonyldiimidazole (CDI), ethylenediamine (EDA), 1-ethyl-3-(3-dimethylaminopropyl)-carbodiimide hydrochloride (EDC), hexafluoro-2-propanol (HFIP), silver nitrate ($AgNO_3$), hydrogen tetrachloroaurate (III) trihydrate ($HAuCl_4{\cdot}3H_2O$), sodium hexachloroplatinate (IV) hexahydrate ($Na_2PtCl_6{\cdot}6H_2O$) and HCA were purchased from Sigma-Aldrich. Milli-Q water was used as deionized water in all experiments.

2.2. Synthesis of Catechol-Grafted Poly(vinyl alcohol). Two grams (45.5 mmol) of PVA were dissolved in 80 mL of dimethyl sulfoxide (DMSO) at 50 °C, and 2.95 g (18.2 mmol) of CDI were dissolved in 15 mL of DMSO at room temperature with magnetic stirring. The CDI solution was added to the PVA solution in a dropwise manner and stirred at room temperature for 3 h. After the activation of CDI, 12.2 mL (182 mmol) EDA was slowly added to the CDI-activated PVA solution and stirred at 50 °C for 24 h. After several precipitations in butanol to remove unreacted reagents, the EDA-modified PVA was dried in vacuo. The intermediate product was purified by dialysis (MWCO = 3.5 kDa, SpectraPor) in deionized water for 3 days and then freeze-dried. The EDA-modified PVA was dissolved in 200 mL of deionized water at pH 5, after which a mixture of 1.16 g (6.38 mmol) of HCA and 2.12 g (13.66 mmol) of EDC in 50 mL deionized water was added to the EDA-modified PVA solution. The pH of the solution was adjusted to 5.5. After 12 h, the final product was purified by dialysis (MWCO = 12−14 kDa, SpectraPor) against an HCl solution (pH 5.0) for 2 days and deionized water for 4 h. The final product was freeze-dried and kept in a moisture-free desiccator before use.

2.3. Preparation of Noble Metal Nanoparticles with PVA-*g*-ct. Silver and gold nanoparticles were prepared by mixing the PVA-*g*-ct solution with a metal precursor solution. PVA-*g*-ct was dissolved in deionized water at a concentration of 1 mg mL^{-1}. $AgNO_3$ and $HAuCl_4$ were dissolved in deionized water at concentrations of 0.4 and 2 mM, respectively, and then mixed with the PVA-*g*-ct solution at a 1:1 volumetric ratio and incubated for 1 and 6 h, respectively, with mild shaking at room temperature. The final concentrations were 0.2 mM for $AgNO_3$, 1 mM for $HAuCl_4$, and 0.5 mg mL^{-1} for PVA-*g*-ct. After the reaction, the nanoparticles were collected by centrifugation at 10 000 rpm for 20 min, washed twice with an excess amount of deionized water, and then redispersed in deionized water.

2.4. Preparation of Catechol-Grafted PVA Nanofibers. PVA-*g*-ct was dissolved in HFIP with vigorous stirring at room temperature at a concentration of 3 wt %. The PVA-*g*-ct solution was electrospun at a voltage of 18 kV, which was controlled using a voltage generator (CPS-40 K03VIT, Chungpa EMT, Seoul, Republic of Korea). A gastight glass syringe with a stainless steel 22-gauge needle was used with a syringe pump (model 781100, KD Scientific) at a flow rate of 1 mL h^{-1}. The distance between the needle and the collection aluminum plate was fixed at 18 cm. PVA was dissolved in HFIP at a concentration of 3 wt % and was electrospun into nanofibers as described above under the same conditions.

2.5. On-Surface Synthesis of Novel Metal Nanostructures on PVA-*g*-ct Nanofibers. The PVA-*g*-ct nanofibers prepared using the 3 wt % polymer solution were used for the synthesis of metal nanostructures on polymer nanofibers. Approximately 0.5 mg of PVA-g-ct nanofibers were initially immersed in pure methanol for 24 h and were then immersed respectively into 2 mL of 0.2 mM $AgNO_3$ in

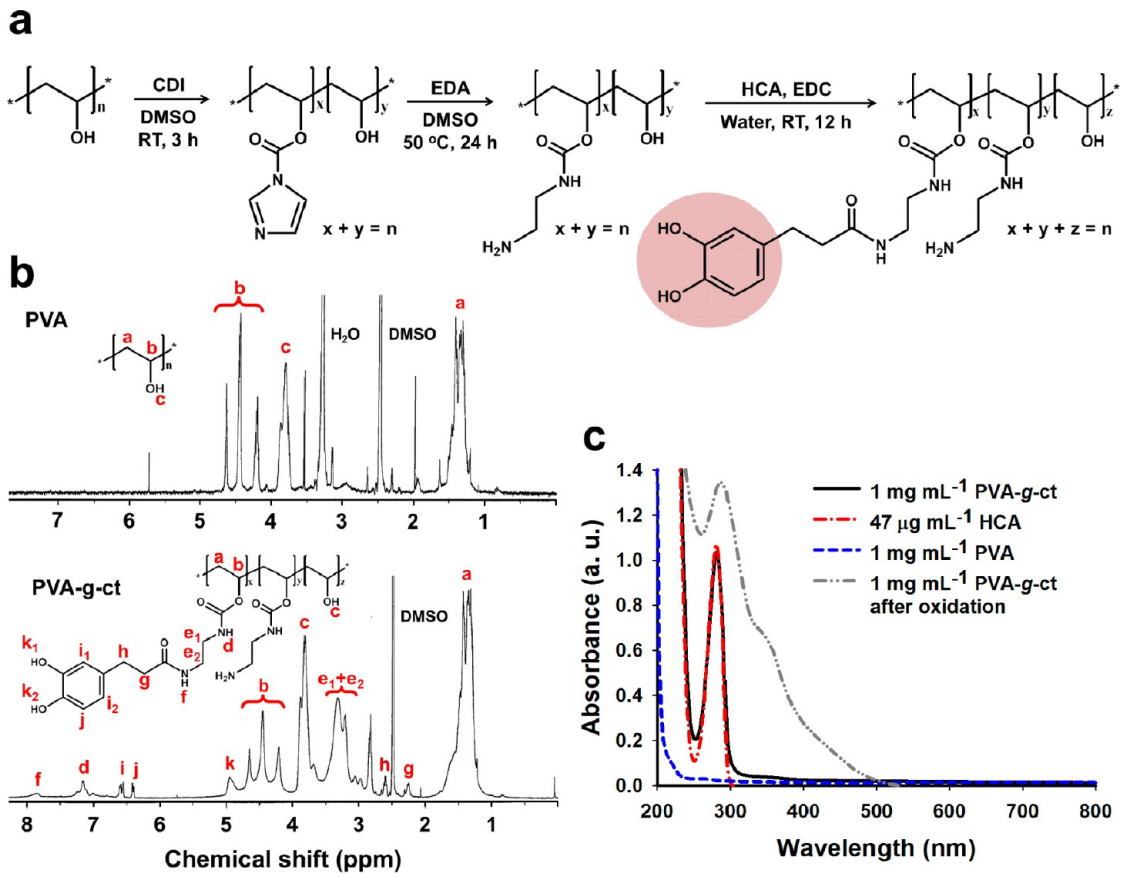

Figure 2. Schematic illustration of the synthesis of (a) catechol-grafted PVA, (b) ^{1}H NMR spectra of PVA (top) and PVA-*g*-ct (bottom) in d_6-DMSO, and (c) light absorption spectra of PVA-*g*-ct, HCA, PVA, and PVA-*g*-ct after oxidation in deionized water at 37 °C for 3 days.

methanol and into a mixture of 0.2 mL of 10 mM $HAuCl_4$ (or Na_2PtCl_6) in deionized water and 1.8 mL of methanol with mild shaking at room temperature. They were then rinsed with an excess amount of methanol and subsequently dried in vacuo. PVA-*g*-ct nanofibers immersed in 1 mM $HAuCl_4$ (orNa_2PtCl_6) solution were calcined in air at 500 °C for 1 h at a heating rate of 10 °C min^{-1}. Gold (or platinum)−silver hybrid nanostructures were prepared using the PVA-*g*-ct nanofibers, which were immersed in 2 mL of 0.2 mM $AgNO_3$ solution for 40 min at room temperature. After being rinsed with an excess amount of methanol, we immersed the PVA-*g*-ct nanofibers in the $AgNO_3$ solution in a 1 mM $HAuCl_4$ (or Na_2PtCl_6) solution for 1 h (or 2 h) at room temperature.

2.6. Characterization. PVA-*g*-ct was analyzed using nuclear magnetic resonance (^{1}H NMR, Bruker Avance, 400 MHz) and UV−vis spectrophotometry (UV-1601, Shimadzu, Japan). The morphology of the prepared nanofibers was examined with scanning electron microscopy (SEM, Hitachi S-4800, Japan) at an acceleration voltage of 10 kV after coating with platinum to a thickness of about 3 nm. The diameters of the nanofibers were determined from at least 100 sample spots in the SEM images using the Image J software (U.S. National Institute of Health). An elemental analysis was performed by energy dispersive X-ray spectroscopy (EDX). The nanoparticles were observed using transmission electron microscopy (TEM, JEOL JEM-3011 HR, Japan) at an acceleration voltage of 300 kV. A thermogravimetric analysis (TGA, NETZSCH, TG 209 F3, Germany) was performed for the prepared PVA-*g*-ct nanofibers and on those immersed in the 1 mM $HAuCl_4$ (or Na_2PtCl_6) solution at a heating rate of 10 °C min^{-1} in air.

3. RESULTS AND DISCUSSION

PVA-*g*-ct was synthesized by grafting the catechol moiety of HCA onto PVA using EDA as a linker, as schematically described in Figure2a. The hydroxyl groups of PVA were activated with CDI, and the active intermediates were reacted with the primary amine groups of EDA to convert some of the hydroxyl groups of PVA into primary amines.An excessive amount of EDA was added to the CDI-activated PVA solution in order to prevent the intrachain cyclization of PVA.[33,34] The catechol moiety of HCA was grafted onto the EDA-modified PVA using an EDC coupling reaction between the carboxylic acid groups of HCA and the primary amine groups of the EDA-modified PVA.Figure 2b shows the ^{1}H NMR spectra of unmodified PVA and the prepared PVA-*g*-ct. The peaks of the prepared PVA-*g*-ct in the range of 6.4−6.6 ppm indicate the presence of a catechol moiety, whereas no peak appears in the same range of the ^{1}H NMR spectrum of unmodified PVA. The substitution degree of the catechol moiety was about 3.1%, as determined by the ratio of the areas under each peak corresponding to the protons of the catechol moiety and carbon backbone. The presence of the catechol moiety of PVA-*g*-ct was also examined by light absorption spectroscopy (Figure 2c). The absorption peak of catechol at 280 nm appeared in the PVA-*g*-ct solution, which corresponds to the absorption of the HCA solution used for the synthesis of PVA-*g*-ct. After the oxidation of PVA-*g*-ct at 37 °C for 3 days, the absorption wavelength was extended to 500 nm with a small peak at 350 nm due to the oxidation of catechol to quinone, indicating the successful conjugation of the catechol molecules to PVA.

To determine whether PVA-*g*-ct can spontaneously reduce noble metal ions to solid metal nanostructures, an aqueous solution of metal ion precursors ($AgNO_3$, $HAuCl_4$, and Na_2PtCl_6) was mixed with the PVA-*g*-ct solution at room

dx.doi.org/10.1021/am401550p | ACS Appl. Mater. Interfaces 2013, 5, 6381−6390

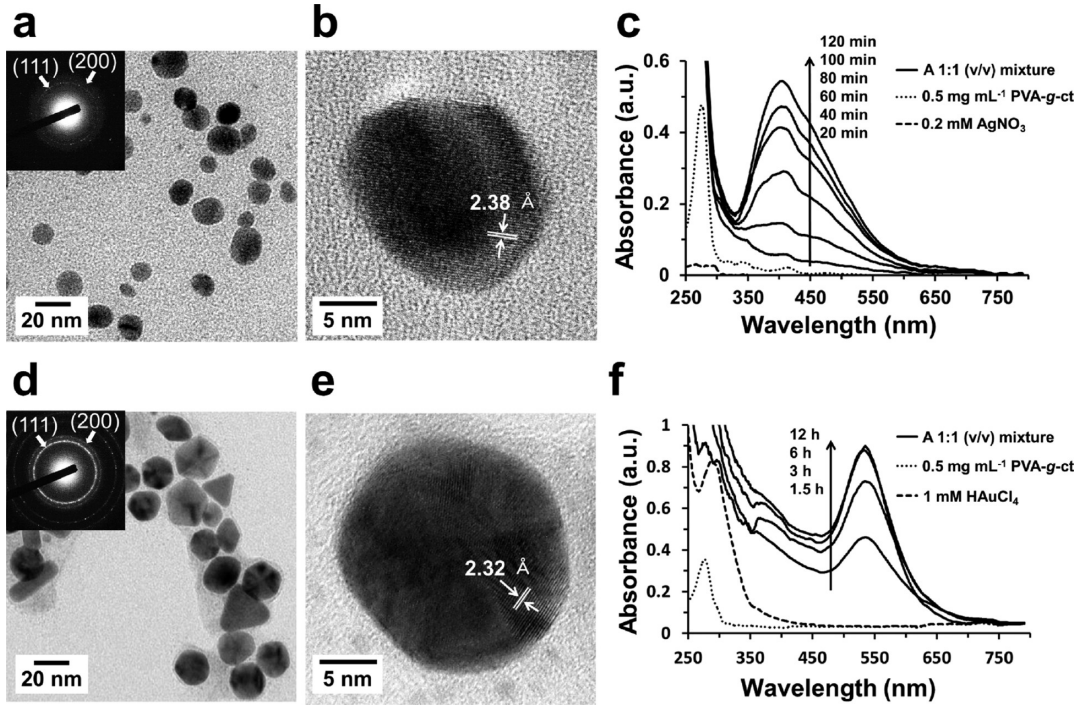

Figure 3. (a) TEM (inset: SAED pattern) and (b) HRTEM images, and (c) absorption spectra of silver nanoparticles, along with (d) TEM (inset: SAED pattern) and (e) HRTEM images and the absorption spectra (f) of gold nanoparticles. The metal nanoparticles were synthesized using a 1:1 (v/v) mixture of 1 mg mL^{-1} of PVA-*g*-ct and a metal ion precursor solution (0.4 mM $AgNO_3$ or 2 mM $HAuCl_4$ in deionized water).

temperature for up to 12 h. A TEM analysis and the light absorption spectra indicate that silver and gold nanoparticles were synthesized simply by mixing the catechol-grafted PVA with the metal precursor solutions without additional reducing agents (Figure 3), whereas no apparent change was observed for the platinum precursor solution (see Figure S1 in the Supporting Information). The redox potential of the platinum ions, $[PtCl_6]^{2-}$, is known to be +680 mV vs NHE, which is lower than these values for Ag^+ (+ 791 mV vs NHE) and $[AuCl_4]^-$ (+1.0 V vs NHE).[35,36] Although the average redox potential of $[PtCl_6]^{2-}$ is more positive than that of catechol (+ 530 mV vs NHE), the complete conversion of the platinum ions into a solid structure requires four sequential reduction steps. At least one of the four reduction steps may require more reduction power; hence,the reduction capability of the catechol moiety may not be enough to reduce the $[PtCl_6]^{2-}$ under ambient conditions. In contrast to the platinum precursor ions, the formation of metal nanoparticles was clearly observed for the silver and gold precursor ions. The average diameters were 11.5 ± 3.1 nm and 21.4 ± 11.2 nm for silver and gold nanoparticles, respectively, as determined from at least 100 sample spots of TEM images. A high-resolution TEM analysis showed that the *d*-spacings of adjacent lattice planes were 2.38 Å and 2.32 Å for silver and gold nanoparticles, respectively. Both correspond to the (111) plane. The surface plasmon resonance (SPR) of silver and gold nanoparticles enabled usto monitor their generation using UV−vis absorption spectroscopy as a function of the reaction time. The SPR peaksclearly appeared around 410 and 540 nm for silver and gold nanoparticles after incubation for 40 and 90 min, respectively. The absorbance increased with anincrease in the incubation time, indicating an increasednumber of nanoparticles exhibiting SPR effects.

Catechol-functionalized polymer nanofibers were prepared by electrospinning a 3 wt % PVA-*g*-ct solution in HFIP. The diameter of PVA-*g*-ct nanofibers was much smaller than that of the PVA nanofibers: they were 561 ± 250 nm and 273 ± 103 nm, respectively. In addition, no significant effect of the polymer concentration on the diameters of the PVA-*g*-ct nanofibers was found. Both of the nanofibers had a broad diameter distribution (see Figure 4), and the variation in the diameter may have been caused by incomplete solvent evaporation and jet splitting during the electrospinning process.[37] In particular, we speculate that the increased

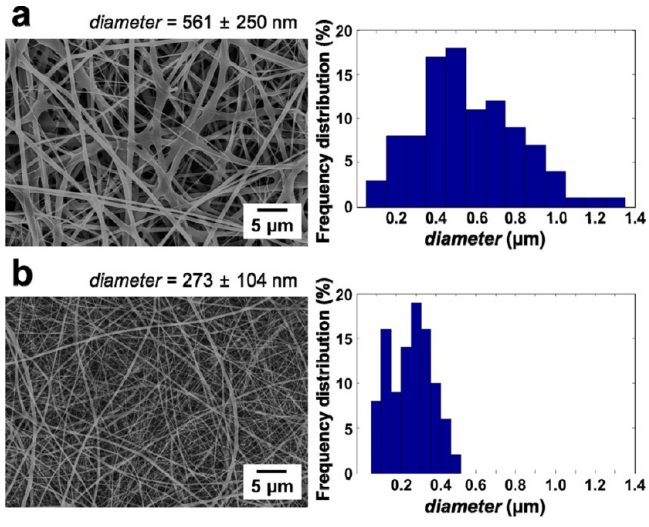

Figure 4. SEM images and size distributions of (a) the electrospun PVA nanofibers and (b) PVA-*g*-ct nanofibers prepared in HFIP at concentrations of 3 wt %. The number above each image indicate the average diameter with standard deviation of at least 100 nanofibers.

cohesive forces of PVA-*g*-ct via the interchain interactions of the grafted catechol molecules may be involved in the increased variation in the properties of the PVA-*g*-ct solution. Further study is now underway to identify the critical factors that determine the diameter and morphology of the electrospun PVA-*g*-ct nanofibers when varying the number of catechols involved in grafting. In this work, we focused on the application of PVA-*g*-ct nanofibers to the templating synthesis of noble metal nanostructures under ambient conditions without using additional highly reactive reducing agents.

The templating synthesis of silver nanoparticles was performed using PVA-*g*-ct nanofibers as a chemically reactive template. Methanol was used as a reaction medium instead of water because PVA-*g*-ct nanofibers are soluble in water and lose their porous structure. The PVA-*g*-ct nanofiber matrix retained the porous structure formed by the nanofibers after incubation with $AgNO_3$ in methanol (Figure 5a, b). Silver nanoparticles

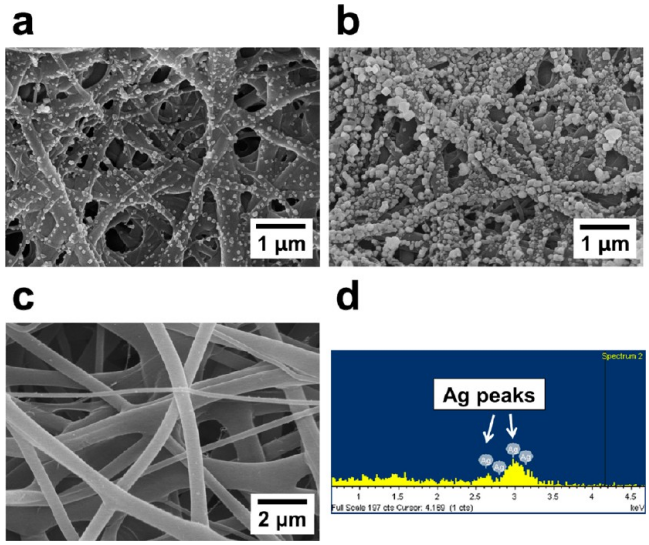

Figure 5. SEM images of the electrospun PVA-*g*-ct nanofibers after incubation with a 0.2 mM $AgNO_3$ in methanol for (a) 20 and (b) 40 min, and the electrospun PVA nanofibers after incubation in the same solution for (c) 40 min. (d) EDX spectrum of electrospun PVA-*g*-ct nanofibers immersed for 40 min.

were spontaneously generated on the surfaces of PVA-*g*-ct nanofibers after only 20 min of incubation with mild shaking at room temperature (Figure 5a), and the number and diameter of silver nanoparticles increased as the incubation time increased: 53.3 ± 12.5 nm for 20 min, 86.2 ± 32.8 nm for 40 min (Figure 5b). In contrast, no solid nanoparticles were generated on the PVA nanofibers, even after incubation for 40 min (Figure 5c), and no silver elements were found in the EDX spectrum. These results confirmed that the PVA nanofibers have no reducing activity for the silver ions. The results also demonstrated that the formation of silver nanoparticles was driven by the oxidation of the catechol moiety in PVA-*g*-ct. The EDX spectrum of the PVA-*g*-ct nanofibers immersed in a 0.2 mM $AgNO_3$solution for 40 min identified the silver element of the nanoparticles generated on the surface of the polymer nanofibers (Figure 5d). In addition, Fourier-transform infrared (FT-IR) spectroscopic analysis shows that the phenolic C−O−H bending vibration (1350 cm^{-1}) and phenolic C−O−H stretching vibration (1290 and 1037 cm^{-1}) of the catechol group in PVA-*g*-ct significantly decreased when the nanofibers were treated with the silver ion precursors. The same decrease was clearly observed for the PVA-*g*-ct nanofibers treated with 0.2 mM NaOH under the same conditions, indicating that the oxidation of the catechol moiety in PVA-*g*-ct are responsible for the reduction of the silver ions into solid silver nanoparticles.

Figure 6 shows the formation of gold nanoparticles on PVA-*g*-ct nanofibers by immersing the nanofibers in a 1 mM $HAuCl_4$ solution at an ambient temperature. Some gold nanoparticles with a diameter of 28.4 ± 9.4 nm were spontaneously generated on the PVA-*g*-ct nanofibers; however, the number of the particles was much smaller than the silver nanoparticles on the same polymer nanofibers (Figure 6a, b). In our experiments, it was found that the color of the gold precursor solution incubated with the PVA-*g*-ct nanofibers changed from light yellow to colorless, indicating that the gold precursor ions were reduced to a lower oxidation state, whereas the color of the PVA-*g*-ct nanofibers changed from white to wine red, indicating the formation of gold nanoparticles on the PVA-*g*-ct nanofibers. Because the complete reduction of the gold precursor ions requires three electron transfers, the density of the catechol groups is critical for the reduction of gold ions to metallic gold nanoparticles. A limited number of the catechol groups exposed to the nanofibers could result in the incomplete reduction of gold ions. The EDX spectrum of PVA-*g*-ct nanofibers immersed in a 1 mM $HAuCl_4$ solution for 12 h showed the coexistence of gold and chloride on the polymer nanofibers (see Figure S2 in the Supporting Information), indicating that the gold ions reduced to a lower oxidation state were complexed with the catechol moieties of the PVA-*g*-ct nanofibers but were not completely reduced to metallic gold nanoparticles. A TGA analysis supported the presence of gold ions combined with PVA-*g*-ct nanofibers, as it showed that most of the as-prepared PVA-*g*-ct nanofibers were removed, whereas the residual weight of the PVA-*g*-ct nanofibers with 1 mM $HAuCl_4$ at 800 °C was about 29% (Figure 6f). The calcination of the PVA-*g*-ct nanofibers complexed with gold ions at 500 °C for 1 h induced the further reduction of the complexed gold ions into solid metal nanostructures, as shown in images c and d in Figure 6. An EDX analysis also indicated that the gold ions were completely reduced to metallic gold nanoparticles by thermal reduction (Figure 6e). Highly porous gold nanostructures were formed with interconnected gold nanoparticles along the polymer nanofiber structures. The large particles with 98.0 ± 22.6 nm in diameter resulted from the growth of the pregenerated gold nanoparticles, and the small nanoparticles with 20.9 ± 5.3 nm in diameter resulted from the thermal reduction of the complexed gold ions during the calcination process. The interconnected small nanoparticles enable the morphology and porosity of the as-prepared electrospun polymer nanofibers to be retained, whereas the silver nanoparticles on the PVA-g-ct nanofibers were aggregated after calcination (see Figure S3 in the Supporting Information). Note that the gold nanoparticles and nanostructures were generated on the PVA-*g*-ct nanofibers despite the fact that the nanofibers were rinsed with pure methanol several times before calcination. This result indicates that the gold ions are stably coordinated with the catechol groups of the PVA-*g*-ct nanofibers. Therefore, although the oxidation of catechols of the PVA-*g*-ct nanofibers was high enough to generatethe silver nanoparticles without an additional treatment, the gold ions were only partially reduced and complexed with the catechol groups, presumably because of the relatively low density of the catechol groups, requiring an additional thermal treatment for

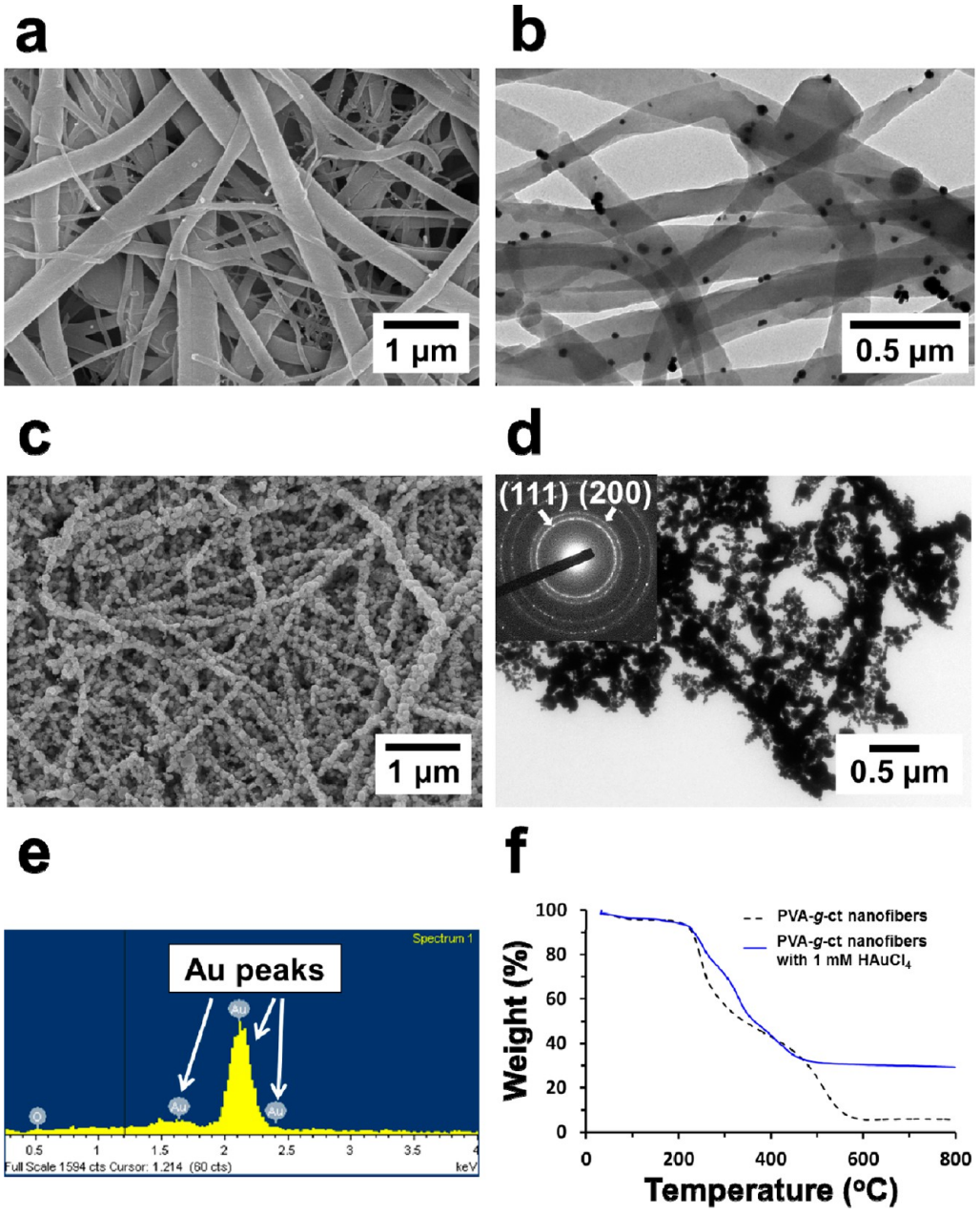

Figure 6. (a) SEM and (b) TEM images of the electrospun PVA-*g*-ct nanofibers immersed in a 1 mM $HAuCl_4$ solution for 12 h at room temperature. (c) SEM image, (d) TEM image (inset: SAED pattern), and (e) EDX spectrum after calcination at 500 °C for 1 h. (f) TGA thermograms of PVA-*g*-ct nanofibers and PVA-*g*-ct nanofibers immersed in a 1 mM $HAuCl_4$ solution for 12 h at room temperature.

the complete reduction of the complexed gold ions into metallic gold nanostructures.

We also synthesized nanofiber-templated platinum nanostructures following the same procedures, i.e., by immersing the PVA-*g*-ct nanofibers in 1 mM Na_2PtCl_6 at room temperature. No observable platinum nanoparticles were generated on the PVA-*g*-ct nanofibers, though the contrast of their TEM image without staining increased remarkably, presumably because of the complexation of the platinum ions with the polymer nanofibers (Figure 7a, b). The color of the PVA-*g*-ct nanofibers changed from white to brown after immersing the nanofibers in the 1 mM Na_2PtCl_6 solution,indicating that the platinum precursor ions were partially reduced and complexed with the PVA-*g*-ct nanofibers but not completely reduced to platinum nanoparticles, similar to the gold precursor ions. The EDX spectrum of the PVA-*g*-ct nanofibers immersed in the 1 mM Na_2PtCl_6 solution for 12 h showed the coexistence of platinum and chloride on the polymer nanofibers (see Figure S4 in the Supporting Information). Furthermore, the TGA analysis showed that the residual weight of the PVA-*g*-ct nanofibers incubated with the platinum precursor solution was about 24% at 800 °C, indicating that the partially reduced platinum ions were strongly bonded to the PVA-*g*-ct nanofibers (Figure 7f). The PVA-*g*-ct nanofibers immersed in the 1 mM Na_2PtCl_6 solution were also calcined at 500 °C for 1 h. Electron microscopic analyses with electron diffraction and EDX showed that the calcination process generated a very rough and porous metallic platinum nanofiber structure from the PVA-*g*-ct nanofibers complexed with platinum ions (Figure 7c–e).

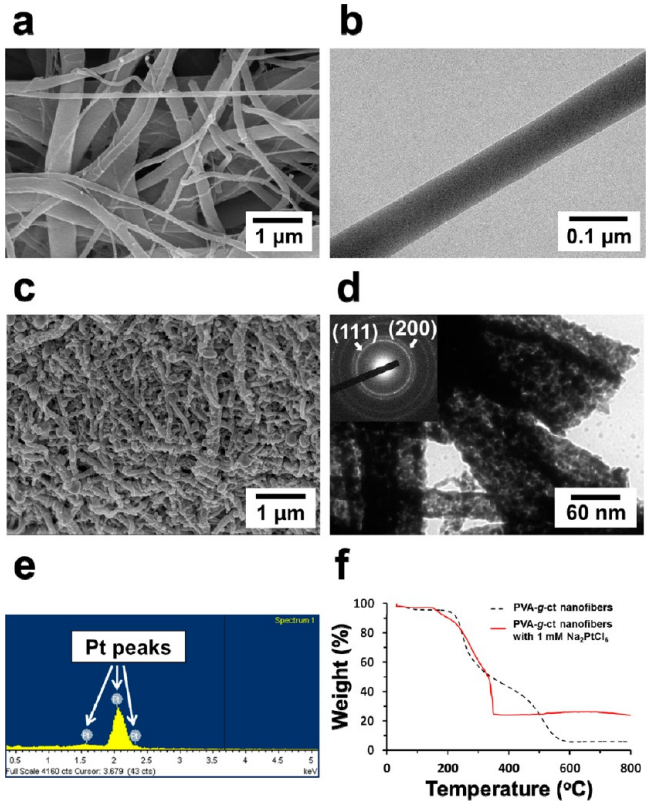

Figure 7. (a) SEM and (b) TEM images of the electrospun PVA-*g*-ct nanofibers immersed in a 1 mM Na_2PtCl_6 solution for 12 h at room temperature. (c) SEM image, (d) TEM image (inset: SAED pattern), and (e) EDX spectrum after calcination at 500 °C for 1 h. (f) TGA thermograms of PVA-*g*-ct nanofibers and PVA-*g*-ct nanofibers immersed in a 1 mM Na_2PtCl_6 solution for 12 h at room temperature.

Next, we attempted the nanofiber templating synthesis of multimetallic hybrid nanostructures by harnessing the presynthesized silver nanoparticles on the PVA-*g*-ct nanofibers to induce the reduction of gold and platinum ions via a galvanic replacement method.[38,39] Figure 8 shows the PVA-*g*-ct nanofibers immersed in a 0.2 mM $AgNO_3$ solution followed by incubation with a 1 mM $HAuCl_4$solution. An EDX analysis showed the coexistence of silver and gold elements along with chloride peaks. Particularly, several clusters of gold nanoparticles were overlapped with relatively large silver nanostructures, indicating that the gold nanoparticles were generated on the surface of themetallic silver structures. Interestingly, tiny gold nanoparticles (~2 nm in diameter) were also spontaneously generated on the nanofibers, though no such particles were observed without the silver nanoparticles. This result suggests that the presence of the silver nanoparticles assisted with the formation of the gold nanoparticles. The precise underlying mechanism that led to the reduction of the gold ions in the presence of both metallic silver and catechols immobilized on the same substrate is not clear yet. We speculate that some gold ions partially reduced by the silver nanoparticles may have been nucleated on the surface of the PVA-*g*-ct nanofibers, producing tiny metallic nanostructures. The formation of gold nanoclusters on the metallic silver surface could also be facilitated by the catechol-mediated partial reduction of the gold ions. The chloride signals may result from both of the formation of solid AgCl during the replacement reaction and the partially reduced gold ions coordinated with the polymer nanofibers.[38] It was found that the tiny gold nanoparticles were generated on the surface of the PVA-*g*-ct nanofibers, as shown in Figure 8b. Elemental mappings show that the large nanoparticles consisted of silver and that the gold nanoparticles covered the surface of the PVA-*g*-ct nanofibers as well as the silver nanoparticles (Figure 8e). These results indicate that the remaining catechols on the surface of PVA-*g*-ct nanofibers can reduce the gold ions more effectively in the presence of silver nanoparticles. Simultaneously, some of the gold ions were reduced on the silver nanoparticles through galvanic replacement. The silver nanoparticles were completely converted to gold nanoparticles after incubation with the 1 mM $HAuCl_4$ solution for 12 h (Figure 8f, g).

We also examined the conversion of the silver nanoparticles on the PVA-*g*-ct nanofibers into platinum nanostructures via galvanic replacement. The PVA-*g*-ct nanofibers were immersed in a 0.2 mM $AgNO_3$ solution and then transferred to a 1 mM Na_2PtCl_6 solution. Figure 9 shows the coexistence of silver and platinum on the PVA-*g*-ct nanofibers. Platinum nanoparticles were generated on the silver nanoparticles and on the surfaces of PVA-*g*-ct nanofibers, as observed during the formation of gold nanoparticles on the PVA-*g*-ct nanofibers. The galvanic replacement of metallic silver byplatinum ions cannot occur theoretically due to the lower redox potential of $PtCl_6^{2-}$ compared to that of Ag^+, as mentioned above. However, as briefly mentioned above regarding the reduction of gold ions in the presence of the silver nanoparticles, the platinum ions (Pt^{n+}) could be partially reduced by the catechols remaining on the PVA-*g*-ct nanofibers, thus enabling the galvanic replacement reaction between silver nanoparticles and platinum ions.[39] The silver nanoparticles were completely replaced by the platinum ions after incubation with 1 mM Na_2PtCl_6 for 12 h (Figure 9e, f). Therefore, the silver nanoparticles on the catechol-functionalized substrates can mediate the formation of gold and platinum nanostructures without calcination, and the silver contents of the metal nanostructures can be controlled by the duration of the reaction time.

4. CONCLUSION

This study introduced catechol-grafted polymer nanofibers as a reactive template for the synthesis and immobilization of noble metal nanostructures. The synthesis of gold, silver, and platinum nanostructures was driven by the oxidation of the catechol moiety, which was chemically grafted to the PVA backbone. PVA-*g*-ct was electrospun into nanofibers, and the prepared PVA-*g*-ct nanofibers were used as templates for metal nanostructures. The templating synthesis of individual noble metal nanoparticles showed that the reducing capability of the PVA-*g*-ct nanofibers was high enough for the spontaneous and complete reduction of silver ions to metallic nanostructures under ambient conditions, whereas gold and platinum ions were only partially reduced because the reduction of these materials requires multiple electron transfers. However, both of the metal ions were strongly complexed with the catechol moieties of the PVA-*g*-ct nanofiber, allowing additional processing for further reactions. Very rough gold and platinum nanostructures were generated on the nanofiber templates by a calcination process. The presynthesis of the silver nanoparticles on the PVA-*g*-ct nanofibers enabled the formation of silver–gold and silver–platinum hybrid nanostructures because of galvanic replacement and possibly the reductive microenvironments provided by the catechol groups when exposed to the surface of the nanofibers. This facile synthesis method

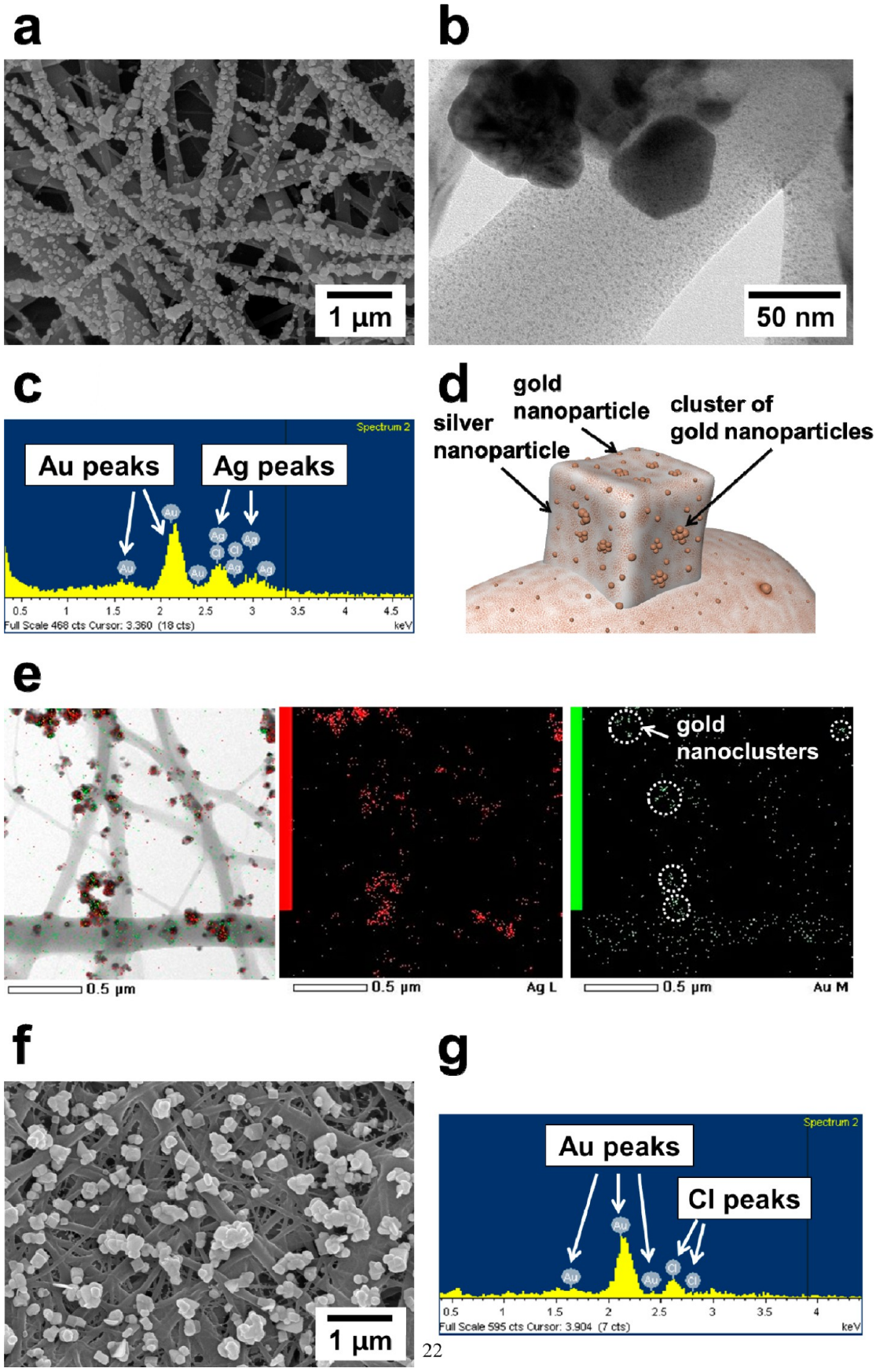

22

Figure 8. (a) SEM image, (b) TEM image, (c) EDX spectrum, (d) schematic illustration, and (e) elemental mappings (red, silver; green, gold) of the PVA-*g*-ct nanofibers immersed in 0.2 mM $AgNO_3$ solution for 40 min followed by immersion in a 1 mM $HAuCl_4$ solution for 1 h at room temperature. (f) SEM image and (g) EDX spectrum after further immersion in the 1 mM $HAuCl_4$ solution.

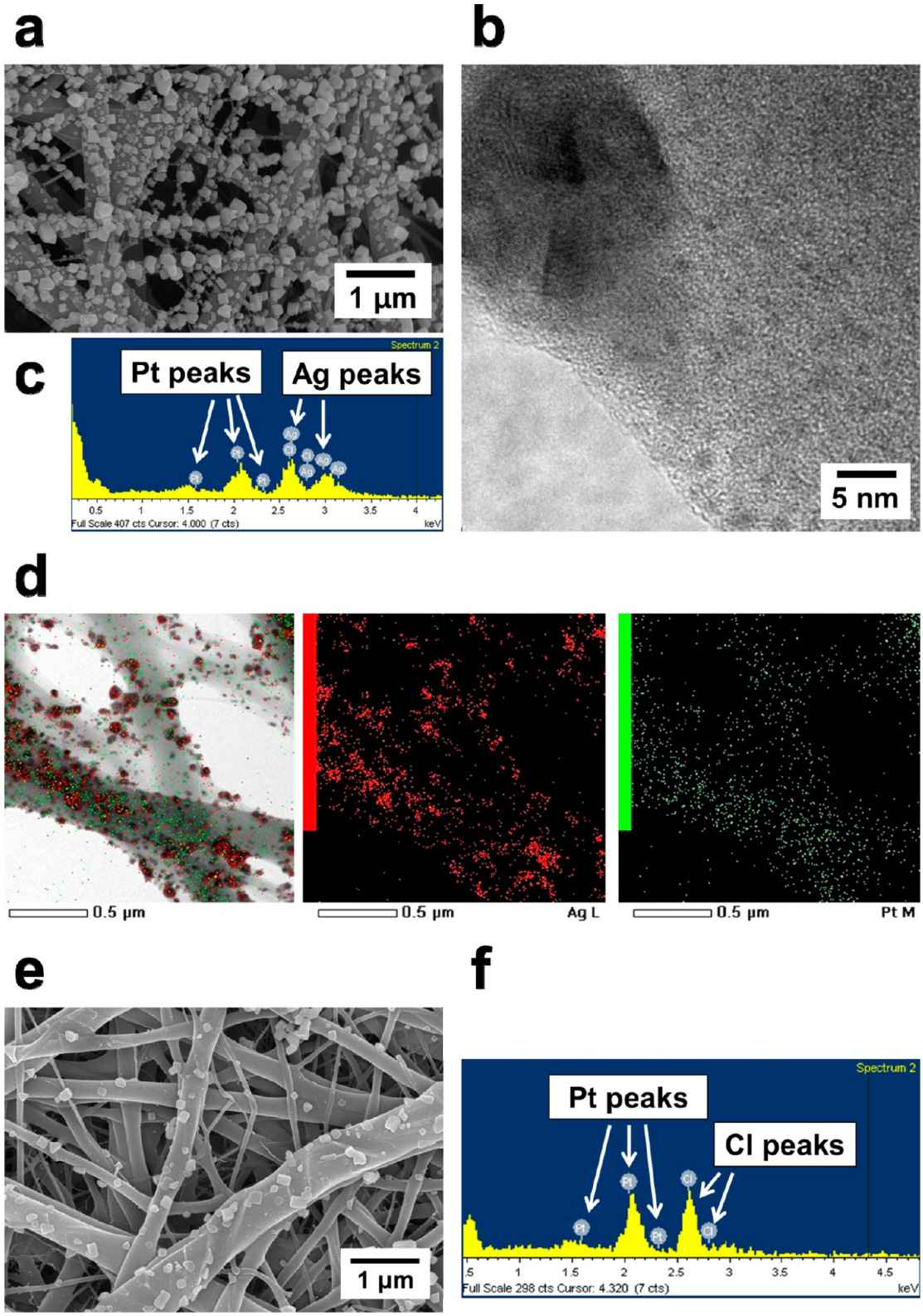

Figure 9. (a) SEM image, (b) TEM image, (c) EDX spectrum, and (d) elemental mappings (red, silver; green, platinum) of the PVA-*g*-ct nanofibers immersed in a 0.2 mM $AgNO_3$ solution for 40 min followed by immersion in a 1 mM Na_2PtCl_6 solution for 2 h at room temperature. (e) SEM image and (f) EDX spectrum after further immersion in the 1 mM Na_2PtCl_6 solution.

generates metal nanoparticles and unique metal nanostructures with three-dimensional porous structures that can be used for a wide range of applications, such as sensors, catalytic systems, electronic and optical devices, and tissue engineering. This work also demonstrated unique advantages of our mussel-inspired chemistry approach for the preparation of functional inorganic−organic hybrid nanofibers. For instance, for the polymer solution for electrospinning, no metal precursor salts

dx.doi.org/10.1021/am401550p | *ACS Appl. Mater. Interfaces* 2013, 5, 6381−6390

need to be added. In our process, polymer nanofibers are first electrospun, and then metal precursor ions are incorporated for in situ mineralization. This difference makes a significant advantage because the electrospinning procedures can be optimized without metal ions; otherwise, detailed experimental conditions need to be adjusted, which depends on the kind of metal ions and their concentrations because the addition of metal ions can change the optimal conditions of electrospinning. In addition, multiple materials can be incorporated to polymer nanofibers in a controlled manner. The catechol moiety is very well-known to have a strong affinity toward metal oxides. Therefore, metal oxide nanoparticles can be coassembled with metal nanoparticles, producing multicomponent, more complex nanostructures. The application of these advantageous features to the synthesis of functional hybrid nanomaterials is now under investigation.

■ ASSOCIATED CONTENT

Ⓢ Supporting Information

The absorption spectra of the platinum precursor solution mixed with the PVA-*g*-ct solution as well as additional SEM and TEM images and the EDX spectra. This material is available free of charge via the Internet at http://pubs.acs.org.

■ AUTHOR INFORMATION

Corresponding Author

*E-mail: haeshin@kaist.ac.kr (H.L.); yoonsung@kaist.ac.kr (Y.S.N.).

Notes

The authors declare no competing financial interest.

■ ACKNOWLEDGMENTS

This work was supported under the framework of the international cooperation program managed by National Research Foundation of Korea (2012K2A1A2033167) and by Korea Biotech R&D Program (2012K001398). We also appreciate Mr. Insu Kim for his technical assistance.

■ REFERENCES

(1) Xia, Y.; Yang, P.; Sun, Y.; Wu, Y.; Mayers, B.; Gates, B.; Yin, Y.; Kim, F.; Yan, H. *Adv. Mater.* **2003**, *15*, 353−389.
(2) Zheng, H.; Li, Y.; Liu, H.; Yin, X.; Li, Y. *Chem. Soc. Rev.* **2011**, *40*, 4506−4524.
(3) White, R. J.; Luque, R.; Budarin, V. L.; Clark, J. H.; Macquarrie, D. J. *Chem. Soc. Rev.* **2009**, *38*, 481−494.
(4) Bell, A. T. *Science* **2003**, *299*, 1688−1691.
(5) Tanabe, I.; Tatsuma, T. *Nano Lett.* **2012**, *12*, 5418−5421.
(6) Nam, Y. S.; Park, T. G. *J. Biomed. Mater. Res.* **1999**, *47*, 8−17.
(7) Nam, Y. S.; Park, T. G. *Biomaterials* **1999**, *20*, 1783−1790.
(8) Hou, Q.; Grijpma, D. W.; Feijen, J. *Biomaterials* **2003**, *24*, 1937−1947.
(9) Nam, Y. S.; Yoon, J. J.; Park, T. G. *J. Biomed. Mater. Res.* **2000**, *53*, 1−7.
(10) Johnson, S. A.; Ollivier, P. J.; Mallouk, T. E. *Science* **1999**, *283*, 963−965.
(11) Li, D.; Xia, Y. *Adv. Mater.* **2004**, *16*, 1151−1170.
(12) Lee, J. A.; Nam, Y. S.; Rutledge, G. C.; Hammond, P. T. *Adv. Funct. Mater.* **2010**, *20*, 2424−2429.
(13) Song, J.; Chen, M.; Regina, V. R.; Wang, C.; Meyer, R. L.; Xie, E.; Wang, C.; Besenbacher, F.; Dong, M. *Adv. Eng. Mater.* **2012**, *14*, B240−B246.
(14) Ouyang, L.; Dotzauer, D. M.; Hogg, S. R.; Macanás, J.; Lahitte, J.-F.; Bruening, M. L. *Catal. Today* **2010**, *156*, 100−106.
(15) Dotzauer, D. M.; Dai, J.; Sun, L.; Bruening, M. L. *Nano Lett.* **2006**, *6*, 2268−2272.
(16) Müller, K.; Quinn, J. F.; Johnston, A. P. R.; Becker, M.; Greiner, A.; Caruso, F. *Chem. Mater.* **2006**, *18*, 2397−2403.
(17) Dong, H.; Wang, D.; Sun, G.; Hinestroza, J. P. *Chem. Mater.* **2008**, *20*, 6627−6632.
(18) Carlberg, B.; Ye, L.-L.; Liu, J. *Small* **2011**, *7*, 3057−3066.
(19) Fang, X.; Ma, H.; Xiao, S.; Shen, M.; Guo, R.; Cao, X.; Shi, X. *J. Mater. Chem.* **2011**, *21*, 4493−4501.
(20) Lee, H.; Dellatore, S. M.; Miller, W. M.; Messersmith, P. B. *Science* **2007**, *318*, 426−430.
(21) Ryu, J. H.; Lee, Y.; Kong, W. H.; Kim, T. G.; Park, T. G.; Lee, H. *Biomacromolecules* **2011**, *12*, 2653−2659.
(22) Ham, H. O.; Liu, Z.; Lau, K. H. A.; Lee, H.; Messersmith, P. B. *Angew. Chem., Int. Ed.* **2011**, *50*, 732−736.
(23) Cui, J.; Yan, Y.; Such, G. K.; Liang, K.; Ochs, C. J.; Postma, A.; Caruso, F. *Biomacromolecules* **2012**, *13*, 2225−2228.
(24) Ye, Q.; Zhou, F.; Liu, W. *Chem. Soc. Rev.* **2011**, *40*, 4244−4258.
(25) Hong, S.; Lee, J. S.; Ryu, J.; Lee, S. H.; Lee, D. Y.; Kim, D. P.; Park, C. B.; Lee, H. *Nanotechnology* **2011**, *22*, 494020.
(26) Hwang, D. S.; Harrington, M. J.; Lu, Q.; Masic, A.; Zeng, H.; Waite, J. H. *J. Mater. Chem.* **2012**, *22*, 15530−15533.
(27) Steenken, S.; Neta, P. *J. Phys. Chem.* **1982**, *86*, 3661−3667.
(28) Lee, Y.; Park, T. G. *Langmuir* **2011**, *27*, 2965−2971.
(29) Black, K. C. L.; Liu, Z.; Messersmith, P. B. *Chem. Mater.* **2011**, *23*, 1130−1135.
(30) Son, H. Y.; Ryu, J. H.; Lee, H.; Nam, Y. S. *Macromol. Mater. Eng.* **2013**, *298*, 547−554.
(31) Fullenkamp, D. E.; Rivera, J. G.; Gong, Y.; Lau, K. H. A.; He, L.; Varshney, R.; Messersmith, P. B. *Biomaterials* **2012**, *33*, 3783−3791.
(32) Abargues, R.; Gradess, R.; Canet-Ferrer, J.; Abderrafi, K.; Valdes, J. L.; Martinez-Pastor, J. *New J. Chem.* **2009**, *33*, 913−917.
(33) Kakinoki, A.; Kaneo, Y.; Ikeda, Y.; Tanaka, T.; Fujita, K. *Biol. Pharm. Bull.* **2008**, *31*, 103−110.
(34) Kakinoki, A.; Kaneo, Y.; Tanaka, T.; Hosokawa, Y. *Biol. Pharm. Bull.* **2008**, *31*, 963−969.
(35) Liu, L.; Pippel, E. *Angew. Chem., Int. Ed.* **2011**, *50*, 2729−2733.
(36) Yang, Z.; Tseng, W.-L.; Lin, Y.-W.; Chang, H.-T. *J. Mater. Chem.* **2005**, *15*, 2450−2454.
(37) Zhang, F.; Zuo, B. Q.; Zhang, H. X.; Bai, L. *Polymer* **2009**, *50*, 279−285.
(38) Sun, Y.; Xia, Y. *J. Am. Chem. Soc.* **2004**, *126*, 3892−3901.
(39) Kim, M. R.; Lee, D. K.; Jang, D.-J. *Appl. Catal., B* **2011**, *103*, 253−260.